









Polycomb group ring finger protein 6 suppresses Myc-induced lymphomagenesis

Nina Tanaskovic¹ , Mattia Dalsass¹ , Marco Filipuzzi¹, Giorgia Ceccotti¹, Alessandro Verrecchia¹ , Paola Nicoli¹, Mirko Doni¹ , Daniela Olivero² , Diego Pasini^{1,3}, Haruhiko Koseki^{4,5} , Arianna Sabò¹, Andrea Bisso¹ , Bruno Amati¹ 

Max is an obligate dimerization partner for the Myc transcription factors and for several repressors, such as Mnt, Mxd1-4, and Mga, collectively thought to antagonize Myc function in transcription and oncogenesis. Mga, in particular, is part of the variant Polycomb group repressive complex PRC1.6. Here, we show that ablation of the distinct PRC1.6 subunit Pcgf6—but not Mga—accelerates Myc-induced lymphomagenesis in Eμ-myc transgenic mice. Unexpectedly, however, Pcgf6 loss shows no significant impact on transcriptional profiles, in neither pre-tumoral B-cells, nor lymphomas. Altogether, these data unravel an unforeseen, Mga- and PRC1.6-independent tumor suppressor activity of Pcgf6.

DOI [10.26508/lsa.202101344](https://doi.org/10.26508/lsa.202101344) | Received 17 December 2021 | Revised 4 April 2022 | Accepted 4 April 2022 | Published online 14 April 2022

Introduction

The Myc-Max network is constituted by a set of transcription factors that dimerize and bind DNA via a common basic-helix-loop-helix-leucine zipper motif (bHLH-LZ). Max is a key node in this network, acting as an obligate dimerization partner for proteins of the Myc (c-, N- and L-Myc) and Mxd/Mga subfamilies (Mxd1-4, Mnt, and Mga), which activate and repress transcription, respectively, by binding to the same consensus DNA element, the E-box CACGTG and variants thereof (Carroll et al, 2018). Mxd1-4 and Mnt share a short N-terminal domain responsible for recruitment of mSin3/HDAC corepressor complexes. Mga lacks this domain but was independently identified—together with Max—as a component of the variant Polycomb group (PcG) repressive complex PRC1.6, characterized by the presence of two distinct PcG- and E2F-family proteins (respectively, Pcgf6 and E2f6) (Ogawa et al, 2002; Gao et al, 2012; Carroll et al, 2018; Llabata et al, 2020). In mouse embryonic stem cells (mESCs), depletion of Mga led to dissociation of other PRC1.6

subunits (Pcgf6, E2f6 and L3mbtl2) from chromatin (Endoh et al, 2017; Stielow et al, 2018; Scelfo et al, 2019). Along the same line, depletion of Pcgf6 caused dissociation of several subunits (Ring1A/B and Rybp), whereas others (Mga, Max, and L3mbtl2) remained chromatin-bound (Zhao et al, 2017). Altogether, these findings suggest that Mga/Max and Pcgf6 contribute to the hierarchical assembly of the PRC1.6 complex onto chromatin, may thereby counteract transcriptional activation by Myc and E2F at common target genes, and thus also their growth-promoting and oncogenic activities.

A number of observations pointed to a tumor suppressor function of the Mga/Max dimer. First, genome sequencing studies revealed loss-of-function mutations in Mga in a wide variety of tumors (Schaub et al, 2018). Loss of Max was also observed, but appears to be restricted to neuroendocrine tumors, including pheochromocytoma (Comino-Mendez et al, 2011; Burnichon et al, 2012) and small-cell lung cancer (SCLC) (Romero et al, 2014; Llabata et al, 2021). In SCLC, mutations affecting the different network members (Max loss, Mga loss, Myc amplification) occur in a mutually exclusive manner, pointing to a common functional consequence (Romero et al, 2014). Formal evidence for this hypothesis was provided in two SCLC mouse models, in which deletion of Max could either abrogate tumorigenesis if combined with a MYCL transgene, or favor it after loss of the Rb1 and Trp53 tumors suppressors (Augert et al, 2020). Hence, in neuroendocrine tumors loss of Mga/Max/PRC1.6 repressor function may be sufficient to bypass the requirement for Myc activity, as recently shown in Max-null human SCLC cell lines (Llabata et al, 2021). In other lineages, the essential role of Max as a Myc partner (Amati et al, 1993) may prevent its loss, but may still co-exist with its antagonist activities in complex with either Mga or Mxd/Mnt proteins. In line with these observations, loss of Mga in a murine Myc-proficient non-small-cell lung cancer model accelerated tumor growth and caused de-repression of PRC1.6, E2F, and Myc/Max target genes (Mathsyaraja et al, 2021).

¹European Institute of Oncology (IEO) - IRCCS, Milan, Italy ²Laboratorio Analisi Veterinarie BiEsseA, A Company of Scil Animal Care Company Srl, Milan, Italy ³Department of Health Sciences, University of Milan, Milan, Italy ⁴Laboratory of Developmental Genetics, RIKEN Center for Integrative Medical Sciences, Yokohama, Japan ⁵Cellular and Molecular Medicine, Advanced Research Departments, Graduate School of Medicine, Chiba University, Chiba, Japan

Correspondence: bissoand81@gmail.com; bruno.amati@ieo.it
 Nina Tanaskovic's present address is Postbiotica Srl, Milan, Italy
 Mattia Dalsass's present address is Department CIBIO, University of Trento, Trento, Italy
 Arianna Sabò's present address is QUANTRO Therapeutics GmbH, Vienna, Austria
 Andrea Bisso's present address is Gadeta BV, Utrecht, The Netherlands

Recurrent mutations in *Mga* were also reported in lymphoid malignancies, including Natural Killer/T-cell lymphoma (NKTCL) (Zhang et al, 2018; Kim & Ko, 2022), Chronic Lymphoid Leukemia (Edelmann et al, 2012; De Paoli et al, 2013; Puente et al, 2015) and diffuse large B-cell lymphoma (DLBCL) (Reddy et al, 2017; Lee et al, 2020). Although *Myc* activation and/or overexpression are widely associated with the progression of these malignancies, it remains to be determined whether *Mga* and the PRC1.6 complex antagonize *Myc* activity in this setting.

Here, we addressed whether loss of either *Mga* or the PRC1.6-restricted subunit *Pcgf6* (Gao et al, 2012) potentiate *Myc*-induced lymphomagenesis in $E\mu$ -*myc* transgenic mice. In previous studies based on the same model, *Max* was essential for lymphomagenesis (Mathsyaraja et al, 2019); more surprisingly, *Mnt* also showed tumor-promoting activity in this model, owing most likely to selective suppression of *Myc*-induced apoptosis (Campbell et al, 2017; Nguyen et al, 2020). Unexpectedly, our data point to a distinct function of *Pcgf6* in tumor suppression, independent from either *Mga*, PRC1.6, or transcriptional control.

Results and Discussion

Loss of *Pcgf6* accelerates *Myc*-induced lymphomagenesis

To address the roles of *Mga* and *Pcgf6* in *Myc*-induced lymphomagenesis, we combined the $E\mu$ -*myc* (Adams et al, 1985) and *CD19-Cre* transgenes (Rickert et al, 1997)—thus expressing both *Myc* and *Cre* recombinase from the pro B-cell stage—with either the conditional knockout alleles *Mga*^{lnv} (hereafter *Mga*^{fl}) (Washkowitz et al, 2015) or *Pcgf6*^{fl} (Endoh et al, 2017) (Table S1). Whereas targeting *Mga* showed no effect (Fig S1A–C), deletion of *Pcgf6* significantly enhanced $E\mu$ -*myc*-dependent lymphomagenesis, with *Pcgf6*^{+fl} and *Pcgf6*^{fl/fl} animals showing progressive reductions in median disease-free survival, and increased disease penetrance (Fig 1A).

Of note, control $E\mu$ -*myc*; *Mga*^{+/+} and $E\mu$ -*myc*; *Pcgf6*^{+/+} animals showed very different kinetics of lymphoma onset, with median disease-free survival times of 203 and 97 d, respectively (Figs 1A and S1A). Such variations are common with the $E\mu$ -*myc* model, whether comparing different studies (e.g., Adams et al [1985], Gorrini et al [2007], and Mathsyaraja et al [2019]), or independent cohorts within the same study as exemplified here, and are most likely attributable to multiple genetic modifiers, especially when the genetic backgrounds intermix as a consequence of the breeding with different alleles. Hence, for each targeted allele, only littermates from the same cohort should be considered as proper “wild-type” controls.

Relative to *Pcgf6*^{+/+} controls, *Pcgf6*^{+fl} and *Pcgf6*^{fl/fl} tumors (hereafter *Pcgf6*^{+Δ} and *Pcgf6*^{Δ/Δ} or KO) showed proportionate decreases in *Pcgf6* mRNA levels (Fig 1B), and immunoblot analysis confirmed loss of the protein in the latter (Fig 1C). The *Pcgf6* genotype affected neither the differentiation stage of the tumors, with comparable proportions arising from naive mature B-cells (B220⁺ IgM⁺) and B-cell precursors (B220⁺ IgM⁻) (Fig 1D) (Langdon et al, 1986), nor their pathological classification, all examined cases showing DLBCL/Burkitt’s like features (Table S2). Finally, we exploited our RNA-seq profiles (see below) to analyze tumor

clonality through the scoring of reads in the Immunoglobulin heavy chain variable region (Barbosa et al, 2020 Preprint): in contrast with the widespread concept that lymphomas arising in $E\mu$ -*myc* mice are monoclonal, classically based on Southern blotting (Adams et al, 1985) or PCR (Yu & Thomas-Tikhonenko, 2002), we detected multiple clones in most samples (Fig S2 and Table S3), pointing to a more complex oligo- or polyclonal organization of these lymphomas. Most relevant here, our data did not reveal any consistent impact of the *Pcgf6* genotype on clonal complexity, indicating that accelerated tumor onset in the *Pcgf6*^{+fl} and *Pcgf6*^{fl/fl} backgrounds could not simply be ascribed to increased clonality.

Altogether, we conclude that *Pcgf6*, functions as a dose-dependent, haplo-insufficient tumor suppressor in *Myc*-induced lymphomagenesis, without altering the gross pathological and cellular features of the resulting tumors. Unlike *Pcgf6*, *Mga* showed no tumor suppressor activity in $E\mu$ -*myc* mice, pointing to a PRC1.6-independent function of *Pcgf6* in this model.

Loss of *Pcgf6* affects *Myc*-induced apoptosis in B-cells

Young $E\mu$ -*myc* mice show a characteristic expansion of pre-tumoral B-cells, counter-balanced by a concomitant increase in apoptosis (Nilsson et al, 2005). Monitoring of bone marrow B220⁺CD19⁺ B-cells revealed that their fraction was significantly increased in the *Pcgf6*^{fl/fl} background (Fig 2A) correlating with an impairment in *Myc*-induced apoptosis (Fig 2B). In contrast with the effect on apoptosis, loss of *Pcgf6* caused no major alterations in the cell cycle profiles of B220⁺CD19⁺ B cells, in either control or $E\mu$ -*myc* transgenic mice (Fig 2C). Of note, whereas the effect of *Pcgf6* loss on *Myc*-induced lymphomagenesis was already apparent in heterozygous *Pcgf6*^{+fl} mutant mice (Fig 1A), the same was not true for B-cell counts and apoptosis (Fig 2A and B); this apparent discrepancy might be due either to a limiting sensitivity of the pre-tumoral measurements, or to the co-existence of additional mechanisms of tumor suppression by *Pcgf6*. Altogether, our data suggest that the accelerated lymphoma onset in $E\mu$ -*myc*; *CD19-Cre*; *Pcgf6*^{fl/fl} mice may be explained—at least in part—by increased survival at the pre-tumoral stage, which might favor the expansion of the B220⁺CD19⁺ B-cell pool, thus increasing the opportunities for the emergence of tumor clones.

Loss of *Pcgf6* does not affect *Myc*-dependent transcription

As assayed by RNA-seq profiling, pre-tumoral $E\mu$ -*myc* B-cells show characteristic changes in gene expression relative to control non-transgenic B-cells (Sabò et al, 2014). This was confirmed in our cohorts, with separate clustering of control and pre-tumoral samples (respectively C and P, Fig 3A); within each cluster, however, the *Pcgf6*^{+/+} and *Pcgf6*^{fl/fl} genotypes (WT and KO) remained intermingled. At either the C or P stage, calling for differentially expressed genes (DEGs) between the WT and KO samples yielded virtually no changes (Table S4A–C). Taking WT B-cells as a common control, similar numbers of DEGs were called in WT and KO pre-tumoral samples, with a large overlap between the two genotypes (Fig 3B–D and Table S4D and E). Similarly, RNA-seq profiling of tumor samples (T) yielded high correlation indices among all tumors with no clustering according to *Pcgf6* status (Fig S3A), similar

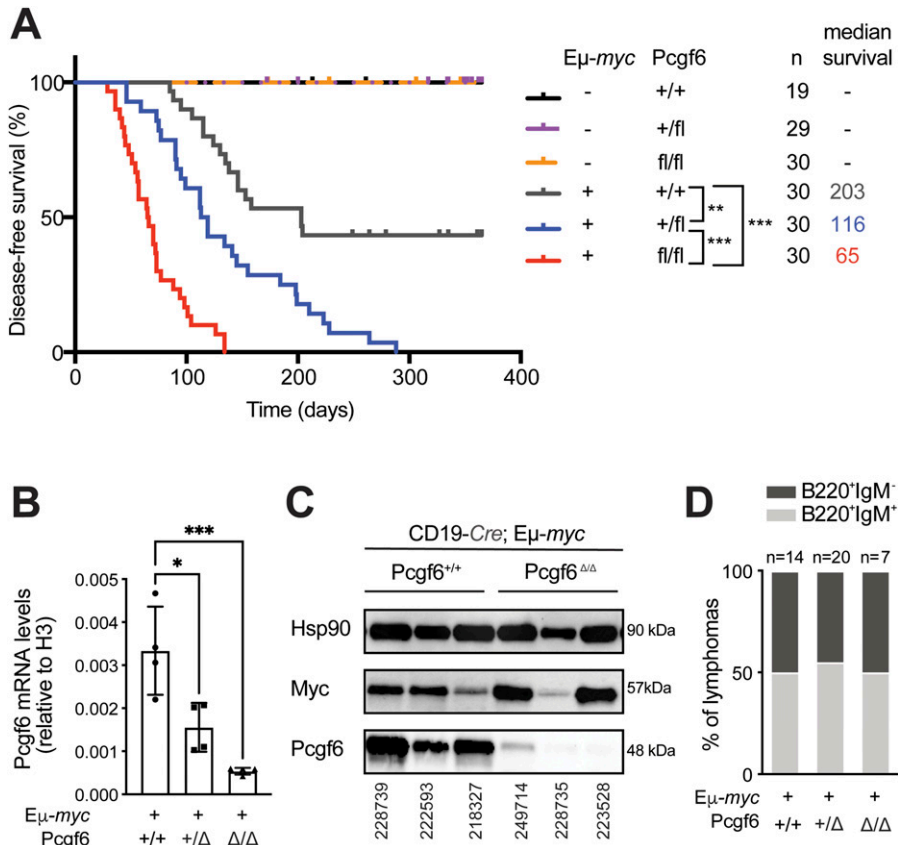


Figure 1. Loss of *Pcgf6* cooperates with *Myc* overexpression in B-cell lymphoma development. (A) Disease-free survival curves for mice of the indicated *Eμ-myc* and *Pcgf6* genotypes (all with the *CD19-Cre* transgene). The number of mice (n) and median survival (in days) are indicated. (B) *Pcgf6* mRNA levels were measured by RT-qPCR on mRNA extracted from sorted *CD19⁺* lymphoma cells, sampled from infiltrated lymph nodes of *CD19-Cre; Eμ-myc* mice, with the indicated *Pcgf6^{f/f}* genotypes. The data show means and s.d.; **P* < 0.05; ***P* < 0.001; ****P* < 0.0001. (C) Western blot analysis of *Pcgf6* and *Myc* protein expression in infiltrated lymph nodes from either *CD19-Cre; Eμ-myc; Pcgf6^{f/+}* or *CD19-Cre; Eμ-myc; Pcgf6^{Δ/Δ}* tumors. *Hsp90* was used as loading control. One representative mouse per genotype is shown and mice IDs are indicated at the bottom. Note that a residual *Pcgf6* signal in *Pcgf6^{Δ/Δ}* samples might be due to infiltrating non-deleted cells. (D) Immunophenotyping of *B220⁺ IgM⁺* reveals similar proportions of *B220⁺ IgM⁺* tumors among *Eμ-myc* lymphomas of the indicated *Pcgf6* genotypes. The numbers above each bar represent number of mice analyzed for each genotype. Source data are available for this figure.

transcriptional changes in the KO and WT tumors relative to control B-cells (Fig S3B) and very few DEGs (84 up and 81 down) in KO relative to WT tumors (Table S4F and Fig S3C). Most noteworthy here, whereas *Pcgf6* was not called as DEG in this comparison, the RNA-seq profiles confirmed the complete absence of *Pcgf6* exons 2 and 3 in KO tumors (Fig S3D). In conclusion, *Pcgf6* impacted neither on steady-state gene expression profiles, nor on *Myc*-dependent responses during B-cell lymphomagenesis.

Although few DEGs were called between *Pcgf6* KO and WT tumors (Fig S3C), these genes might still be relevant to the more aggressive phenotype of the mutant tumors. Gene Ontology analysis of these DEGs (Fig S3E) pointed out several functional categories, among which we noted several immune-related processes among the down-regulated genes. Whether these reflect true differences in gene expression in *Pcgf6* KO versus WT tumor cells or differential infiltration by the host's immune system (e.g., antigen presenting cells, dendritic cells, macrophages, B-, or T-lymphocytes) remains to be determined; nonetheless, these observations suggest that one possible mechanism by which *Pcgf6* suppresses lymphomagenesis may be through modulation of anti-tumoral immune responses.

Most noteworthy here, the action of *Pcgf6* in *Myc*-induced lymphoma is opposite to that of *Pcgf4* (or *Bmi1*), a component of the canonical PRC1 complex (Scelfo et al, 2015) that has pro-tumoral activity in *Eμ-myc* mice, mediated by repression of the tumor suppressor locus *Cdkn2a* (or *Ink4/Arf*) (Jacobs et al, 1999). *Pcgf6* was

also reported to antagonize the function of another canonical PRC1 subunit, *Pcgf2*, in anterior-posterior (A-P) specification during embryogenesis (Endoh et al, 2017). By analogy, the tumor suppressor activity or *Pcgf6* might have been mediated by suppression of canonical PRC1 activity. However, our RNA-seq data did not support this hypothesis: *Cdkn2a* was expressed at very low levels in control B-cells and was de-repressed in pre-tumoral *Eμ-myc* B-cells, as previously described (Eischen et al, 1999), but loss of *Pcgf6* did not reverse this effect (Fig S3F). Together with its limited impact on global expression profiles, these observations suggest that *Pcgf6* does not function as an antagonist of canonical PRC1 during lymphomagenesis.

Mga-dependent recruitment of *Pcgf6* to active chromatin

At first sight, the limited impact of *Pcgf6* on transcriptional profiles appears at odds with its known function as a component of the PRC1.6 complex. The latter should depend on *Mga*, which is required both for the integrity of PRC1.6 and for the recruitment of *Pcgf6* to chromatin, as shown in mESCs and lung tumor cells (Gao et al, 2012; Endoh et al, 2017; Stielow et al, 2018; Scelfo et al, 2019; Mathsyaraja et al, 2021). To address the status of PRC1.6 in our lymphomas, we derived primary lymphoma cultures from *Eμ-myc* control mice and their *Mga^{-/-}* and *Pcgf6^{-/-}* counterparts (Fig S4A). We then used these cells for ChIP-seq profiling of *Pcgf6*, alongside active histone marks (H3K4me3, H3K4me1, and H3K27ac), as well as the PRC2- and

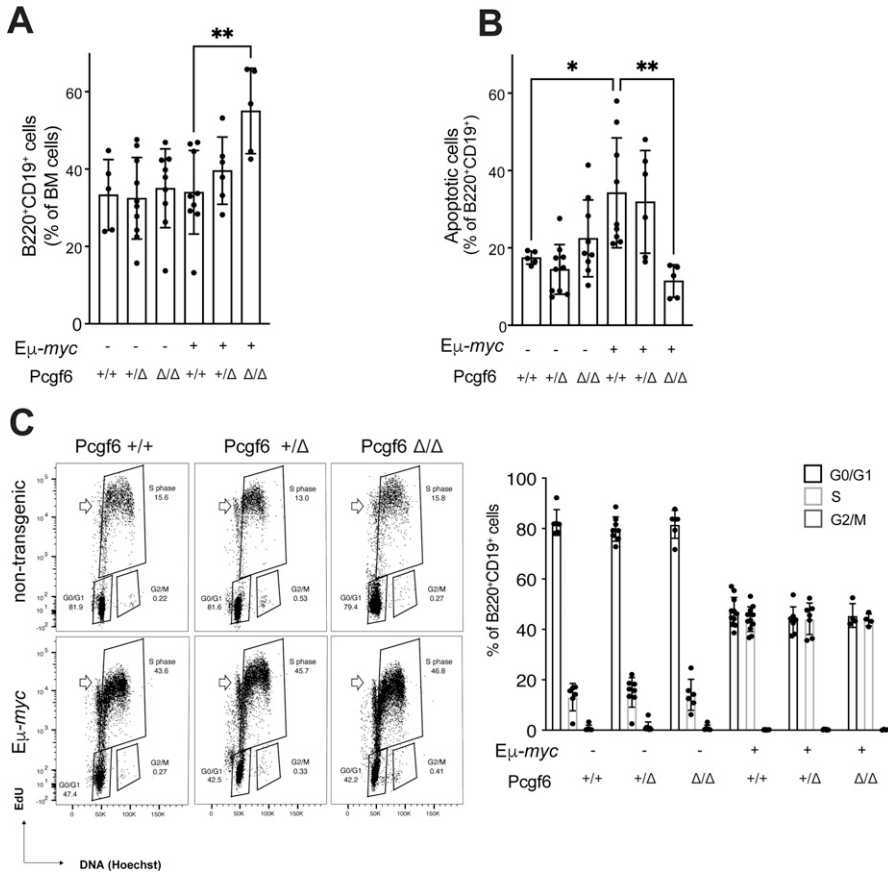


Figure 2. Pcgf6 loss affects Myc-induced apoptosis, but not proliferation in bone marrow B-cells.

(A) Fraction of B220⁺ CD19⁺ cells in the bone marrow (BM) of the indicated experimental groups. **(B)** Fraction of apoptotic B220⁺ CD19⁺ cells, based on Red-VAD-FMK staining for caspase activity. In both panels, the data show means and s.d.; * $P < 0.05$; ** $P < 0.001$. **(C)** Representative EdU/Hoechst flow cytometric profiles of bone marrow-derived B220⁺ CD19⁺ cells in animals of the indicated genotypes. Note that a 2 h EdU pulse in vivo was sufficient for part of the cells to incorporate the nucleotide and complete mitosis, and thus be back in G1 (i.e., with 2N DNA content), whereas scoring as EdU-positive (empty arrowheads): as illustrated here, these cells were neither included in our S-phase gating, nor computed in our G0/G1 counts. Together with the low numbers of cells scored in G2/M, the data imply that B220⁺ CD19⁺ B-cells in vivo undergo mitosis as soon as completing S-phase, with virtually no, or a very short G2 phase. The plot on the right summarizes the data from multiple animals ($n \geq 6$).

PRC1-associated repressive marks H3K27me3 and H2AK119Ub (Di Croce & Helin, 2013).

The distribution of ChIP-seq reads among annotated promoters and distal sites in the genome (Fig S4B), confirmed two of key features established in previous studies. First, the Pcgf6 signal observed in the control $E\mu$ -myc lymphoma was lost not only in $Pcgf6^{-/-}$, but also in $Mga^{-/-}$ cells, in line with the role of Mga in recruiting Pcgf6 to chromatin. Second, Pcgf6 did not co-localize with the PRC-associated marks H3K27me3 and H2AK119Ub but showed preferential binding to active chromatin, as previously observed in mESCs (Stielow et al, 2018; Scelfo et al, 2019). Most relevant here, the propensity to widely associate with active regulatory elements (promoters and enhancers) is a fundamental feature shared by many transcriptional regulators, including Myc/Max and Mga/Max/PRC1.6 complexes (Gao et al, 2012; Sabò et al, 2014; Kress et al, 2016; Endoh et al, 2017; Stielow et al, 2018; Scelfo et al, 2019; Mathsyaraja et al, 2021). As documented for Myc, this initial non-specific engagement of the factor on DNA is insufficient to drive transcription, but is a prerequisite for sequence (i.e., E-box) recognition and establishment of its characteristic gene-regulatory patterns (Sabò & Amati, 2014; Kress et al, 2015; Pellanda et al, 2021). Hence, widespread association with active chromatin—as documented here for Pcgf6—should not be taken to reflect a general role in transcription.

Of note here, one of the apparent changes observed in the $Pcgf6^{-/-}$ lymphoma was an increase in the H3K27Ac signal on

chromatin, at both proximal and distal sites (Fig S4B). However, owing to the small number of Pcgf6- and Mga-null lymphoma cell lines available in our work, as well as to the limiting availability of compound $E\mu$ -myc; $Pcgf6^{fl/fl}$ mice (Table S1), which precluded ChIP-seq analysis in pre-tumoral B-cells (Sabò et al, 2014), we could not determine whether this reflected a real effect of Pcgf6 on H3K27Ac, or a spurious difference—possibly due to clonal variability among lymphomas. For the same reasons, we were unable to address whether loss of PRC1.6 activity might impact Myc's binding profiles in our model. This scenario appears unlikely, however, given that Pcgf6 loss showed no significant impact on Myc-associated gene expression profiles (Figs 3 and S3).

Altogether, whereas Pcgf6 shows Mga-dependent DNA binding, as expected in the context of the PRC1.6 complex, its deletion does not significantly impact transcriptional programs in either control B-cells, pre-tumoral $E\mu$ -myc B-cells, or lymphomas: whether PRC1.6 has a redundant function in transcriptional control or is involved in some other level of chromatin regulation in B-cells remains to be addressed.

Conclusions and future perspectives

In this work, we unravel a distinct tumor suppressor activity of Pcgf6 in Myc-induced lymphomagenesis, unlinked from Mga and the PRC1.6 complex—and possibly from any direct role in gene regulation. These findings warrant thorough characterization of

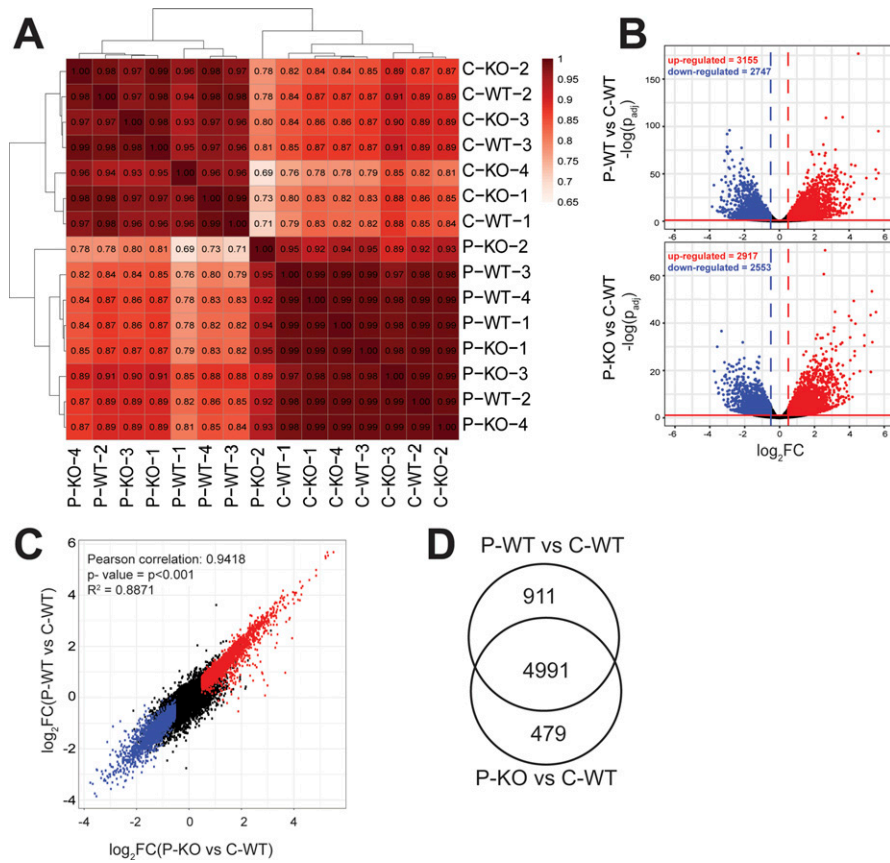


Figure 3. Pcgf6 loss does not affect Myc-dependent transcription.

RNA-seq profiles were generated from control (non-transgenic) and pre-tumoral $E\mu$ -myc B-cells (labeled C and P, respectively) with either *Pcgf6*^{+/+} (WT) or *Pcgf6*^{Δ/Δ} (KO) genotypes. All samples are indicated by the stage (C or P) followed by the *Pcgf6* genotype (WT or KO) and the sample number. For C-WT, n = 3; C-KO, P-WT, and P-KO, n = 4. **(A)** Pairwise Pearson correlation between all samples, based on their RNA-seq profiles. **(B)** Volcano plots showing the differentially expressed genes (DEGs) called in P-WT (top) or P-KO (bottom) with C-WT as a common control. The horizontal and vertical lines within the plots mark the statistical criteria used for calling DEGs, indicating the thresholds for significance ($P_{\text{adj}} < 0.05$) and fold change ($|\log_2\text{FC}| > 0.5$). Up- and down-regulated DEGs are shown in red and blue, respectively, and their numbers indicated at the top. All DEGs are listed in Table S4. **(B, C)** Comparison of the DEGs called in P-WT (Y-axis) and P-KO (X-axis), as defined in (B). The DEGs are colored based on the call in the x-axis. $R^2 = 0.8871$ represents the coefficient of determination. **(D)** Venn diagram showing the overlap in DEGs called in P-WT and P-KO.

alternative *Pcgf6* activities and of their relevance in human tumors: indeed, besides the PRC1.6 complex, *Pcgf6* interacts with the histone H3K4 demethylases JARID1c/d (Lee et al, 2007; Boukhaled et al, 2016) and may have additional partners, yet to be investigated.

Most importantly, our data do not formally rule out a role for *Mga/Max* and PRC1.6 in antagonizing *Myc/Max*-dependent transcription in other tumor types, including DLBCL. In particular, the combination of $E\mu$ -myc and *CD19-Cre*, targeting *Mga*^{f/f}, may not reproduce the more mature activated B-cell (ABC) DLBCL subtype in which *Mga* mutations were reported (Reddy et al, 2017)—although we note that a subset of $E\mu$ -myc tumors do show ABC-like expression profiles (Schleich et al, 2020). Moreover, the oncogenic activation of *Myc*, as modeled by the $E\mu$ -myc transgene, might conceivably be sufficient to overcome the repressive function of *Mga*: in ABC-type DLBCL, in which *MYC* translocation is relatively infrequent (Reddy et al, 2017; Bisso et al, 2019), *Myc* activity may well be antagonized by *Mga*, underlying the selective pressure to inactivate it. Resolving this question would imply the joint scoring of *MYC* translocations and *Mga* mutations in a sizeable number of DLBCL samples, well above those reported so far (125 cases, of which 42 with *MYC* rearrangements and 7 with *MGA* mutations) (Reddy et al, 2017). Finally, any of the five *Mxd/Mnt* proteins that form alternative dimers with *Max* may also contribute repressive activity on common *Mga*- and *Myc*-target genes, and the balance between all these factors may differ

between cell/tumor subtypes, experimental models and/or clinical cases.

Altogether, the contribution of the *Mga/Max*-PRC1.6 complex to DLBCL pathogenesis remains to be addressed. This notwithstanding, our data in the $E\mu$ -myc model establish that in conditions in which *Mga* shows no obvious impact, *Pcgf6* deletion clearly accelerates *Myc*-induced lymphomagenesis.

Materials and Methods

Mouse strains and genotyping

Mice bearing the conditional allele *Mga*^f (originally called *Mga*^{Inv}) (Washkowitz et al, 2015) were bred with either *CD19-Cre* (Rickert et al, 1997) (a gift of Klaus Rajewsky) or $E\mu$ -myc transgenic animals (Adams et al, 1985), and the resulting compound mice bred to obtain the *Mga*-targeted cohort. The same strategy was pursued with the *Pcgf6*^f allele (Endoh et al, 2017). The final crosses used to obtain our experimental cohorts are reported in Table S1. Of note, the *Pcgf6*^f cohort was inbred C57BL/6J, whereas the *Mga*^{f/f} cohort was of mixed genetic background (Washkowitz et al, 2015). In all experiments, gender- and age-matched mice (both females and males) were used without randomization or blinding. Genomic DNA extraction and genotyping were performed as previously described (Bisso et al, 2020), with the PCR primers listed in Table S5.

μ -myc transgenic mice were monitored two to three times a week for tumor development by visual inspection and peripheral lymph node palpation, and were euthanized as soon as they showed signs of lymphoma (i.e., enlarged lymph nodes) (Adams et al, 1985). For pre-tumoral analysis, mice were collected at 4–6 wk of age: spleen and bone marrow were dissected and processed for molecular analysis as previously described (Campaner et al, 2010).

Experiments involving animals were carried out in accordance with the Italian Laws (D.lgs. 26/2014), which enforces Dir. 2010/63/EU (Directive 2010/63/EU of the European Parliament and of the Council of 22 September 2010 on the protection of animals used for scientific purposes) and authorized by the Italian Minister of Health with projects 391/2018-PR.

Isolation and culturing of primary murine lymphoma cell lines

Mice were inspected personally for tumor development. Infiltrated lymph nodes, spleen and bone marrow were collected and smashed in PBS. Cell suspensions were passed three times through a Falcon 70 μ m Cell Strainer (#352350; Corning), centrifuged (80g for 5 min) and resuspended in 10 ml of Erythrocyte Lysis buffer (150 mM NH_4Cl , 10 mM KHCO_3 , and 0.1 mM EDTA). After another centrifugation step, cells were resuspended in 10 ml of MACS buffer (PBS, 2 mM EDTA, and 0.5% BSA), and part of the cells used for in vitro culture. Primary cells were grown in suspension in B-cell medium composed of a 1:1 ratio of DMEM (ECM0103L; Euroclone) and IMDM (I3390; Sigma-Aldrich), supplemented with 10% fetal calf serum (Globefarm Ltd.), 2 mM L-glutamine (Invitrogen Life Technologies), 1% non-essential amino acids (NEAAs), 1% penicillin/streptomycin and 25 μ M β -mercaptoethanol. A lymphoma cell line was considered as stabilized when the splitting ratio reached 1:10 every 2 d, which usually occurred upon 2 wk of in vitro culture.

Analysis of apoptosis, proliferation, and surface markers

Apoptosis in bone marrow-derived B-cells was measured with the CaspGLOW Red Active Caspase Staining Kit (#K190; BioVision) following the manufacturer's guidelines. Proliferation was quantified by EdU staining: EdU (#A10044; Invitrogen) was dissolved in sterile PBS to a concentration of 5 mg/ml; for in vivo proliferation studies, 1 mg EdU in a volume of 200 μ l was injected intraperitoneally 2 h before analysis, followed by staining with the 647 EdU Click Proliferation kit (#565456; BD Pharmingen) according to manufacturer's guidelines. Samples were stained with Hoechst DNA content dye, acquired on a FACSCelesta cytofluorimeter, and analyzed using FlowJo Version 10.4.0 software.

For staining of surface markers, cells were incubated in MACS buffer with fluorochrome-conjugated antibodies (used at the dilutions indicated in Table S5) for at least 1 h at 4°C in the dark, and analyzed by flow cytometry, as above.

Immunoblotting

Protein extraction and immunoblotting were performed as previously described (Bisso et al, 2020) with the indicated primary antibodies (Table S5).

Hematoxylin and Eosin staining

For hematoxylin and eosin staining and pathological analysis tissues were collected and processed as follows. Freshly isolated lymphoma samples were washed in PBS, fixed in 4% (vol/vol) paraformaldehyde at 4°C degrees for at least 16–24 h, washed in PBS, and stored in 70% ethanol at 4°C for a maximum of 1 wk before inclusion. For the latter, each tissue was dehydrated with increasing concentrations of ethanol, embedded in paraffin blocks and stored at RT. For hematoxylin and eosin staining each block was cut into 3/5-mm thick sections and mounted on glass slides. Slides were counterstained with Harris Hematoxylin (#HHS80; Sigma-Aldrich) and Eosin Y solution (#HT110216; Sigma-Aldrich), dehydrated through alcoholic scale, and mounted with Eukitt (#09-00250; Bio-Optica). All images were acquired with the Aperio Digital Pathology Slide Scanner ScanScopeXT (Leica) before pathological evaluation.

RNA sequencing

RNA extraction, processing, and sequencing, as well as the filtering of RNA-seq reads and bioinformatic and statistical analyses, were performed as previously described (Tesi et al, 2019; Bisso et al, 2020; Pellanda et al, 2021). The analysis of tumor clonality from RNA-seq reads was performed as previously described (Barbosa et al, 2020 Preprint).

ChIP sequencing

The fixation of in vitro stabilized lymphoma cell lines and their processing for chromatin immunoprecipitation (ChIP) was performed as previously described (Sabò et al, 2014). 5 μ g of each of the antibodies listed in Table S5 were used to immunoprecipitate either 500 μ g (for the mapping of Myc, Max and Pcgf6) or 250 μ g of fixed chromatin (for the histone marks H3K4me3, H3K4me1, H3K27ac, H3K27me3, and H2Ak119Ub). Whereas Myc and Max precipitates were processed exactly as in Sabò et al (2014), Pcgf6 and histone mark precipitates were processed as in Scelfo et al (2019). 1.5–2 ng of DNA was then used to generate the chromatin immunoprecipitation sequencing (ChIP-Seq) libraries according to the Illumina protocol, and sequenced with the Illumina NovaSeq 6000.

ChIP-seq reads were analyzed as previously published (Sabò et al, 2014; Pellanda et al, 2021). Peaks were mapped and annotated according to the genomic position of their midpoint, as (i) promoter: between –2 and +1 Kb from the annotated refgene start coordinate or transcriptional start site (TSS); (ii) gene body: between >1 Kb from the TSS to the 3' end of an annotated refgene; (iii) intergenic: all peaks positioned outside of the aforementioned intervals. Qualitative and quantitative heatmaps of ChIP-seq enrichment were generated using R with Bioconductor and compEpiTools packages, tools for computational epigenomics (Gentleman et al, 2004; Kishore et al, 2015).

Oligonucleotide primers

Primers for mRNA analysis were designed with Primer-BLAST (<https://www.ncbi.nlm.nih.gov/tools/primer-blast/>) (Ye et al,

2012). The complete list of primers used in this study is shown in Table S5.

Statistical analysis

All experiments were performed at least in biological triplicates. Sample size was not predetermined but is reported in the respective Figure legends. *P*-values were calculated with one-way ANOVA using Tukey correction, except in Fig 1A for Kaplan–Meier survival curves where log *p*-rank test was used.

Data Availability

The RNA-seq data produced in this work have been deposited in NCBI's Gene Expression Omnibus (<https://www.ncbi.nlm.nih.gov/geo/>) and are accessible through the GEO Series accession number GSE190000.

Supplementary Information

Supplementary Information is available at <https://doi.org/10.26508/lsa.202101344>.

Acknowledgements

We thank Stefano Campaner, Francesco Nicassio, Diego Pasini, and members of the Amati lab for discussions, insight, suggestions, and reagents; A Gobbi, M Capillo, and all members of the animal facility for their help with the management of mouse colonies; S Bianchi, L Rotta, T Capra, and L Massimiliano for assistance with Illumina sequencing; S Ronzoni for assistance with flow cytometry; MG Jodice, F Montani, G Bertalot, and S Pece for the help with processing tissue samples; VE Papaioannou for providing *Mga^{fl/fl}* mice; and K Rajewsky for CD19-*Cre* mice. This work was supported by grants from the Italian Health Ministry (RF-2011-02346976), from the Italian Association for Cancer Research (AIRC, IG2015-16768, and IG2018-21594) to B Amati, and from the Ministry of Education, Culture, Sports, Science and Technology of Japan (Grants-in-Aid for Scientific Research, 23249015) to H Kozeki.

Author Contributions

N Tanaskovic: formal analysis, validation, investigation, visualization, and writing—original draft, review, and editing.
M Dalsass: data curation, formal analysis, and visualization.
M Filipuzzi: data curation, formal analysis, visualization, and writing—review and editing.
G Ceccotti: investigation.
A Verrecchia: provided technical support.
P Nicoli: provided technical support.
M Doni: provided technical support.
D Olivero: formal analysis and pathological analysis.
D Pasini: provided *Pcgf6*-mutant mice.
H Koseki: provided *Pcgf6*-mutant mice.
A Sabo: conceptualization, formal analysis, and supervision.
A Bisso: conceptualization, formal analysis, supervision, investigation, and writing—original draft, review, and editing.

B Amati: conceptualization, supervision, funding acquisition, project administration, and writing—original draft, review, and editing.

Conflict of Interest Statement

The authors declare that they have no conflict of interest.

References

- Adams JM, Harris AW, Pinkert CA, Corcoran LM, Alexander WS, Cory S, Palmier RD, Brinster RL (1985) The *c-myc* oncogene driven by immunoglobulin enhancers induces lymphoid malignancy in transgenic mice. *Nature* 318: 533–538. doi:10.1038/318533a0
- Amati B, Brooks MW, Levy N, Littlewood TD, Evan GI, Land H (1993) Oncogenic activity of the *c-Myc* protein requires dimerization with Max. *Cell* 72: 233–245. doi:10.1016/0092-8674(93)90663-b
- Augert A, Mathsyaraja H, Ibrahim AH, Freie B, Geuenich MJ, Cheng PF, Alibeckoff SP, Wu N, Hiatt JB, Basom R, et al (2020) MAX functions as a tumor suppressor and rewires metabolism in small cell lung cancer. *Cancer Cell* 38: 97–114.e7. doi:10.1016/j.ccell.2020.04.016
- Barbosa R, Xu A, D'Andrea D, Copley F, Patel H, Chakravarty P, Clear A, Calaminici M, Janz M, Zhang B, et al (2020) Co-activation of NF- κ B and MYC renders cancer cells addicted to IL6 for survival and phenotypic stability. *BioRxiv*. doi:10.1101/2020.04.12.038414. (Preprint posted April 13, 2020)
- Bisso A, Filipuzzi M, Gamarra Figueroa GP, Brumana G, Biagioni F, Doni M, Ceccotti G, Tanaskovic N, Morelli MJ, Pendino V, et al (2020) Cooperation between MYC and β -catenin in liver tumorigenesis requires yap/taz. *Hepatology* 72: 1430–1443. doi:10.1002/hep.31120
- Bisso A, Sabò A, Amati B (2019) MYC in germinal center-derived lymphomas: Mechanisms and therapeutic opportunities. *Immunol Rev* 288: 178–197. doi:10.1111/imr.12734
- Boukhaled GM, Cordeiro B, Deblois G, Dimitrov V, Bailey SD, Holowka T, Domi A, Guak H, Chiu HH, Everts B, et al (2016) The transcriptional repressor polycomb group factor 6, PCGF6, negatively regulates dendritic cell activation and promotes quiescence. *Cell Rep* 16: 1829–1837. doi:10.1016/j.celrep.2016.07.026
- Burnichon N, Cascón A, Schiavi F, Morales NP, Comino-Méndez I, Abermil N, Inglada-Pérez L, de Cubas AA, Amar L, Barontini M, et al (2012) MAX mutations cause hereditary and sporadic pheochromocytoma and paraganglioma. *Clin Cancer Res* 18: 2828–2837. doi:10.1158/1078-0432.CCR-12-0160
- Campaner S, Doni M, Hydrbring P, Verrecchia A, Bianchi L, Sardella D, Schleker T, Perna D, Tronnorsjö S, Murga M, et al (2010) Cdk2 suppresses cellular senescence induced by the *c-myc* oncogene. *Nat Cell Biol* 12: 54–59. doi:10.1038/ncb2004
- Campbell KJ, Vandenberg CJ, Anstee NS, Hurlin PJ, Cory S (2017) Mnt modulates Myc-driven lymphomagenesis. *Cell Death Differ* 24: 2117–2126. doi:10.1038/cdd.2017.131
- Carroll PA, Freie BW, Mathsyaraja H, Eisenman RN (2018) The MYC transcription factor network: Balancing metabolism, proliferation and oncogenesis. *Front Med* 12: 412–425. doi:10.1007/s11684-018-0650-z
- Comino-Méndez I, Gracia-Aznárez FJ, Schiavi F, Landa I, Leandro-García LJ, Letón R, Honrado E, Ramos-Medina R, Caronia D, Pita G, et al (2011) Exome sequencing identifies MAX mutations as a cause of hereditary pheochromocytoma. *Nat Genet* 43: 663–667. doi:10.1038/ng.861
- De Paoli L, Cerri M, Monti S, Rasi S, Spina V, Brusca G, Greco M, Ciardullo C, Famà R, Cresta S, et al (2013) MGA, a suppressor of MYC, is recurrently

- inactivated in high risk chronic lymphocytic leukemia. *Leuk Lymphoma* 54: 1087–1090. doi:[10.3109/10428194.2012.723706](https://doi.org/10.3109/10428194.2012.723706)
- Di Croce L, Helin K (2013) Transcriptional regulation by Polycomb group proteins. *Nat Struct Mol Biol* 20: 1147–1155. doi:[10.1038/nsmb.2669](https://doi.org/10.1038/nsmb.2669)
- Edelmann J, Holzmann K, Miller F, Winkler D, Bühler A, Zenz T, Bullinger L, Kühn MW, Gerhardinger A, Bloehdorn J, et al (2012) High-resolution genomic profiling of chronic lymphocytic leukemia reveals new recurrent genomic alterations. *Blood* 120: 4783–4794. doi:[10.1182/blood-2012-04-423517](https://doi.org/10.1182/blood-2012-04-423517)
- Eischen CM, Weber JD, Roussel MF, Sherr CJ, Cleveland JL (1999) Disruption of the ARF-Mdm2-p53 tumor suppressor pathway in Myc-induced lymphomagenesis. *Genes Dev* 13: 2658–2669. doi:[10.1101/gad.13.20.2658](https://doi.org/10.1101/gad.13.20.2658)
- Endoh M, Endo TA, Shinga J, Hayashi K, Farcas A, Ma KW, Ito S, Sharif J, Endoh T, Onaga N, et al (2017) PCGF6-PRC1 suppresses premature differentiation of mouse embryonic stem cells by regulating germ cell-related genes. *Elife* 6: e27970. doi:[10.7554/eLife.21064](https://doi.org/10.7554/eLife.21064)
- Gao Z, Zhang J, Bonasio R, Strino F, Sawai A, Parisi F, Kluger Y, Reinberg D (2012) PCGF homologs, CBX proteins, and RYBP define functionally distinct PRC1 family complexes. *Mol Cell* 45: 344–356. doi:[10.1016/j.molcel.2012.01.002](https://doi.org/10.1016/j.molcel.2012.01.002)
- Gentleman RC, Carey VJ, Bates DM, Bolstad B, Dettling M, Dudoit S, Ellis B, Gautier L, Ge Y, Gentry J, et al (2004) Bioconductor: Open software development for computational biology and bioinformatics. *Genome Biol* 5: R80. doi:[10.1186/gb-2004-5-10-r80](https://doi.org/10.1186/gb-2004-5-10-r80)
- Gorrini C, Squatrito M, Luise C, Syed N, Perna D, Wark L, Martinato F, Sardella D, Verrecchia A, Bennett S, et al (2007) Tip60 is a haplo-insufficient tumour suppressor required for an oncogene-induced DNA damage response. *Nature* 448: 1063–1067. doi:[10.1038/nature06055](https://doi.org/10.1038/nature06055)
- Jacobs JJ, Scheijen B, Voncken JW, Kieboom K, Berns A, van Lohuizen M (1999) Bmi-1 collaborates with c-Myc in tumorigenesis by inhibiting c-Myc-induced apoptosis via INK4a/ARF. *Genes Dev* 13: 2678–2690. doi:[10.1101/gad.13.20.2678](https://doi.org/10.1101/gad.13.20.2678)
- Kim H, Ko YH (2022) The pathologic and genetic characteristics of extranodal NK/T-Cell lymphoma. *Life (Basel)* 12: 73. doi:[10.3390/life12010073](https://doi.org/10.3390/life12010073)
- Kishore K, de Pretis S, Lister R, Morelli MJ, Bianchi V, Amati B, Ecker JR, Pelizzola M (2015) methylPipe and compEpiTools: a suite of R packages for the integrative analysis of epigenomics data. *BMC Bioinformatics* 16: 313. doi:[10.1186/s12859-015-0742-6](https://doi.org/10.1186/s12859-015-0742-6)
- Kress TR, Pellanda P, Pellegrinet L, Bianchi V, Nicoli P, Doni M, Recordati C, Bianchi S, Rotta L, Capra T, et al (2016) Identification of MYC-dependent transcriptional programs in oncogene-addicted liver tumors. *Cancer Res* 76: 3463–3472. doi:[10.1158/0008-5472.CAN-16-0316](https://doi.org/10.1158/0008-5472.CAN-16-0316)
- Kress TR, Sabò A, Amati B (2015) MYC: Connecting selective transcriptional control to global RNA production. *Nat Rev Cancer* 15: 593–607. doi:[10.1038/nrc3984](https://doi.org/10.1038/nrc3984)
- Langdon WY, Harris AW, Cory S, Adams JM (1986) The c-myc oncogene perturbs B lymphocyte development in E-mu-myc transgenic mice. *Cell* 47: 11–18. doi:[10.1016/0092-8674\(86\)90361-2](https://doi.org/10.1016/0092-8674(86)90361-2)
- Lee MG, Norman J, Shilatifard A, Shiekhhattar R (2007) Physical and functional association of a trimethyl H3K4 demethylase and Ring6a/MBLR, a polycomb-like protein. *Cell* 128: 877–887. doi:[10.1016/j.cell.2007.02.004](https://doi.org/10.1016/j.cell.2007.02.004)
- Lee MJ, Koff JL, Switchenko JM, Jhaney CI, Harkins RA, Patel SP, Dave SS, Flowers CR (2020) Genome-defined African ancestry is associated with distinct mutations and worse survival in patients with diffuse large B-cell lymphoma. *Cancer* 126: 3493–3503. doi:[10.1002/ncr.32866](https://doi.org/10.1002/ncr.32866)
- Llabata P, Mitsuishi Y, Choi PS, Cai D, Francis JM, Torres-Diz M, Udeshi ND, Golomb L, Wu Z, Zhou J, et al (2020) Multi-omics analysis identifies MGA as a negative regulator of the MYC pathway in lung adenocarcinoma. *Mol Cancer Res* 18: 574–584. doi:[10.1158/1541-7786.MCR-19-0657](https://doi.org/10.1158/1541-7786.MCR-19-0657)
- Llabata P, Torres-Diz M, Gomez A, Tomas-Daza L, Romero OA, Grego-Bessa J, Llinas-Arias P, Valencia A, Esteller M, Javierre BM, et al (2021) MAX mutant small-cell lung cancers exhibit impaired activities of MGA-dependent noncanonical polycomb repressive complex. *Proc Natl Acad Sci U S A* 118: e2024824118. doi:[10.1073/pnas.2024824118](https://doi.org/10.1073/pnas.2024824118)
- Mathsyaraja H, Catchpole J, Freie B, Eastwood E, Babaeva E, Geuenich M, Cheng PF, Ayers J, Yu M, Wu N, et al (2021) Loss of MGA repression mediated by an atypical polycomb complex promotes tumor progression and invasiveness. *Elife* 10: e64212. doi:[10.7554/eLife.64212](https://doi.org/10.7554/eLife.64212)
- Mathsyaraja H, Freie B, Cheng PF, Babaeva E, Catchpole JT, Janssens D, Henikoff S, Eisenman RN (2019) Max deletion destabilizes MYC protein and abrogates Eμ-Myc lymphomagenesis. *Genes Dev* 33: 1252–1264. doi:[10.1101/gad.325878.119](https://doi.org/10.1101/gad.325878.119)
- Nguyen HV, Vandenberg CJ, Ng AP, Robati MR, Anstee NS, Rimes J, Hawkins ED, Cory S (2020) Development and survival of MYC-driven lymphomas require the MYC antagonist MNT to curb MYC-induced apoptosis. *Blood* 135: 1019–1031. doi:[10.1182/blood.2019003014](https://doi.org/10.1182/blood.2019003014)
- Nilsson JA, Keller UB, Baudino TA, Yang C, Norton S, Old JA, Nilsson LM, Neale G, Kramer DL, Porter CW, et al (2005) Targeting ornithine decarboxylase in Myc-induced lymphomagenesis prevents tumor formation. *Cancer Cell* 7: 433–444. doi:[10.1016/j.ccr.2005.03.036](https://doi.org/10.1016/j.ccr.2005.03.036)
- Ogawa H, Ishiguro K, Gaubatz S, Livingston DM, Nakatani Y (2002) A complex with chromatin modifiers that occupies E2F- and Myc-responsive genes in G0 cells. *Science* 296: 1132–1136. doi:[10.1126/science.1069861](https://doi.org/10.1126/science.1069861)
- Pellanda P, Dalsass M, Filipuzzi M, Loffreda A, Verrecchia A, Castillo Cano V, Thabusot H, Doni M, Morelli MJ, Soucek L, et al (2021) Integrated requirement of non-specific and sequence-specific DNA binding in Myc-driven transcription. *EMBO J* 40: e105464. doi:[10.15252/embj.2020105464](https://doi.org/10.15252/embj.2020105464)
- Puente XS, Beà S, Valdés-Mas R, Villamor N, Gutiérrez-Abril J, Martín-Subero JJ, Munar M, Rubio-Pérez C, Jares P, Aymerich M, et al (2015) Non-coding recurrent mutations in chronic lymphocytic leukaemia. *Nature* 526: 519–524. doi:[10.1038/nature14666](https://doi.org/10.1038/nature14666)
- Reddy A, Zhang J, Davis NS, Moffitt AB, Love CL, Waldrop A, Leppä S, Pasanen A, Meriranta L, Karjalainen-Lindsberg ML, et al (2017) Genetic and functional drivers of diffuse large B cell lymphoma. *Cell* 171: 481–494.e15. doi:[10.1016/j.cell.2017.09.027](https://doi.org/10.1016/j.cell.2017.09.027)
- Rickert RC, Roes J, Rajewsky K (1997) B lymphocyte-specific, Cre-mediated mutagenesis in mice. *Nucleic Acids Res* 25: 1317–1318. doi:[10.1093/nar/25.6.1317](https://doi.org/10.1093/nar/25.6.1317)
- Romero OA, Torres-Diz M, Pros E, Savola S, Gomez A, Moran S, Saez C, Iwakawa R, Villanueva A, Montuenga LM, et al (2014) MAX inactivation in small cell lung cancer disrupts MYC-SWI/SNF programs and is synthetic lethal with BRG1. *Cancer Discov* 4: 292–303. doi:[10.1158/2159-8290.CD-13-0799](https://doi.org/10.1158/2159-8290.CD-13-0799)
- Sabò A, Amati B (2014) Genome recognition by MYC. *Cold Spring Harb Perspect Med* 4: a014191. doi:[10.1101/cshperspect.a014191](https://doi.org/10.1101/cshperspect.a014191)
- Sabò A, Kress TR, Pelizzola M, de Pretis S, Gorski MM, Tesi A, Morelli MJ, Bora P, Doni M, Verrecchia A, et al (2014) Selective transcriptional regulation by Myc in cellular growth control and lymphomagenesis. *Nature* 511: 488–492. doi:[10.1038/nature13537](https://doi.org/10.1038/nature13537)
- Scelfo A, Fernández-Pérez D, Tamburri S, Zanotti M, Lavarone E, Soldi M, Bonaldi T, Ferrari KJ, Pasini D (2019) Functional landscape of PCGF proteins reveals both RING1A/B-Dependent and RING1A/B-Independent-Specific activities. *Mol Cell* 74: 1037–1052.e7. doi:[10.1016/j.molcel.2019.04.002](https://doi.org/10.1016/j.molcel.2019.04.002)
- Scelfo A, Piunti A, Pasini D (2015) The controversial role of the polycomb group proteins in transcription and cancer: How much do we not understand polycomb proteins? *FEBS J* 282: 1703–1722. doi:[10.1111/febs.13112](https://doi.org/10.1111/febs.13112)
- Schaub FX, Dhankani V, Berger AC, Trivedi M, Richardson AB, Shaw R, Zhao W, Zhang X, Ventura A, Liu Y, et al (2018) Pan-cancer alterations of the

- MYC oncogene and its proximal network across the cancer genome atlas. *Cell Syst* 6: 282–300.e2. doi:[10.1016/j.cels.2018.03.003](https://doi.org/10.1016/j.cels.2018.03.003)
- Schleich K, Kase J, Dörr JR, Trescher S, Bhattacharya A, Yu Y, WE M, Fan DYN, Lohneis P, Milanovic M, et al (2020) H3K9me3-mediated epigenetic regulation of senescence in mice predicts outcome of lymphoma patients. *Nat Commun* 11: 3651. doi:[10.1038/s41467-020-17467-z](https://doi.org/10.1038/s41467-020-17467-z)
- Stielow B, Finkernagel F, Stiewe T, Nist A, Suske G (2018) MGA, L3MBTL2 and E2F6 determine genomic binding of the non-canonical Polycomb repressive complex PRC1.6. *PLoS Genet* 14: e1007193. doi:[10.1371/journal.pgen.1007193](https://doi.org/10.1371/journal.pgen.1007193)
- Tesi A, de Pretis S, Furlan M, Filipuzzi M, Morelli MJ, Andronache A, Doni M, Verrecchia A, Pelizzola M, Amati B, et al (2019) An early Myc-dependent transcriptional program orchestrates cell growth during B-cell activation. *EMBO Rep* 20: e47987. doi:[10.15252/embr.201947987](https://doi.org/10.15252/embr.201947987)
- Washkowitz AJ, Schall C, Zhang K, Wurst W, Floss T, Mager J, Papaioannou VE (2015) Mga is essential for the survival of pluripotent cells during peri-implantation development. *Development* 142: 31–40. doi:[10.1242/dev.111104](https://doi.org/10.1242/dev.111104)
- Ye J, Coulouris G, Zaretskaya I, Cutcutache I, Rozen S, Madden TL (2012) Primer-BLAST: A tool to design target-specific primers for polymerase chain reaction. *BMC Bioinformatics* 13: 134. doi:[10.1186/1471-2105-13-134](https://doi.org/10.1186/1471-2105-13-134)
- Yu D, Thomas-Tikhonenko A (2002) A non-transgenic mouse model for B-cell lymphoma: In vivo infection of p53-null bone marrow progenitors by a myc retrovirus is sufficient for tumorigenesis. *Oncogene* 21: 1922–1927. doi:[10.1038/sj.onc.1205244](https://doi.org/10.1038/sj.onc.1205244)
- Zhang Y, Li C, Xue W, Zhang M, Li Z (2018) Frequent mutations in natural killer/T cell lymphoma. *Cell Physiol Biochem* 49: 1–16. doi:[10.1159/000492835](https://doi.org/10.1159/000492835)
- Zhao W, Tong H, Huang Y, Yan Y, Teng H, Xia Y, Jiang Q, Qin J (2017) Essential role for polycomb group protein Pcgf6 in embryonic stem cell maintenance and a noncanonical polycomb repressive complex 1 (PRC1) integrity. *J Biol Chem* 292: 2773–2784. doi:[10.1074/jbc.M116.763961](https://doi.org/10.1074/jbc.M116.763961)



License: This article is available under a Creative Commons License (Attribution 4.0 International, as described at <https://creativecommons.org/licenses/by/4.0/>).